

See discussions, stats, and author profiles for this publication at: <https://www.researchgate.net/publication/286869821>

Title: Control scheme towards enhancing power quality and operational efficiency of single-phase two-stage grid-connected photovoltaic systems

Article in *Journal of Electrical Systems and Information Technology* · December 2015

DOI: 10.1016/j.jesit.2015.05.002

CITATIONS

25

READS

3,035

2 authors:



M.M. Ahmed Salem

Electronics Research Institute

42 PUBLICATIONS 245 CITATIONS

[SEE PROFILE](#)



Yousry Atia

Electronics Research Institute

60 PUBLICATIONS 307 CITATIONS

[SEE PROFILE](#)

Some of the authors of this publication are also working on these related projects:



Design and Implementation of a Single Phase Grid Connected PV System [View project](#)



Grid tie three phase photovoltaic system [View project](#)



Control scheme toward enhancing power quality and operational efficiency of single-phase two-stage grid-connected photovoltaic systems

Mahmoud Salem, Yousry Atia*

Electronics Research Institute, Dokki, Cairo, Egypt

Received 29 March 2015; received in revised form 12 May 2015; accepted 27 May 2015

Abstract

Achieving high reliable grid-connected photovoltaic (PV) systems with high power quality and high operation efficiency is highly required for distributed generation units. A double grid-frequency voltage ripple is found on the dc-link voltage in single-phase photovoltaic grid-connected systems due to the unbalance of the instantaneous dc input and ac output powers. This voltage ripple has undesirable effects on the power quality and operational efficiency of the whole system. Harmonic distortion in the injected current to the grid is one of the problems caused by this double grid-frequency voltage ripple. The double grid frequency ripple propagates to the PV voltage and current which disturb the extracted maximum power from the PV array. This paper introduces intelligent solutions toward mitigate the side effects of the double grid-frequency voltage ripple on the transferred power quality and the operational efficiency of single-phase two-stage grid-connected PV system. The proposed system has three control loops: MPPT control loop, dc-link voltage control loop and inverter current control loop. Solutions are introduced for all the three control loops in the system. The current controller cancels the dc-link voltage effect on the total harmonic distortion of the output current. The dc-link voltage controller is designed to generate a ripple free reference current signal that leads to enhance the quality of the output power. Also a modified MPPT controller is proposed to optimize the extracted power from the PV array. Simulation results show that higher injected power quality is achieved and higher efficiency of the overall system is realized.

© 2015 Electronics Research Institute (ERI). Production and hosting by Elsevier B.V. This is an open access article under the CC BY-NC-ND license (<http://creativecommons.org/licenses/by-nc-nd/4.0/>).

Keywords: Single-phase; Grid-connected; Total harmonic distortion (THD); Photovoltaic; DC-bus control; Maximum power point tracking

1. Introduction

In past few years, penetration of photovoltaic energy resources into the medium and low voltage electricity distribution grid has increased and expected to increase in future due to its economical, technical and environmental benefit

* Corresponding author.

E-mail address: yousry_atia@yahoo.com (Y. Atia).

Peer review under responsibility of Electronics Research Institute (ERI).



<http://dx.doi.org/10.1016/j.jesit.2015.05.002>

2314-7172/© 2015 Electronics Research Institute (ERI). Production and hosting by Elsevier B.V. This is an open access article under the CC BY-NC-ND license (<http://creativecommons.org/licenses/by-nc-nd/4.0/>).

Please cite this article in press as: Salem, M., Atia, Y., Control scheme toward enhancing power quality and operational efficiency of single-phase two-stage grid-connected photovoltaic systems. J. Electr. Syst. Inform. Technol. (2015), <http://dx.doi.org/10.1016/j.jesit.2015.05.002>

(Lal et al., 2013). Single-stage and two-stage grid-connected systems are commonly used topologies in single- and three-phase PV grid connected systems (Du et al., 2014; Yang et al., 2013; Wu et al., 2007; Yang and Smedley, 2008). Two-stage configuration is mainly used because of its advantages of decoupled control since maximum power point tracking (MPPT) control and current injection control are decoupled at different stages. In addition, this gives the freedom to push the switching frequency of the DC–DC converter to an order higher than the inverter stage. As a result, the size and the cost of the converter are decreased (Ahmed et al., 2013). The photovoltaic supply has the feature that the output voltage is widely varying either in DC or AC forms. So a regulated converter is needed to provide stable DC or AC energy (Wang et al., 2007). In two-stage grid connected PV systems, a dc-link capacitor is used to link the two stages. The designer has the flexibility to choose the dc-link voltage and the capacitor size. In single-phase two-stage grid-connected PV system, double grid-frequency voltage ripple can be found on the dc-link voltage because of the unbalance of the instantaneous dc input and ac output powers (Yang et al., 2013; Du et al., 2015). The amplitude of the dc-link voltage ripple can be determined by the selected dc-link voltage, the dc-link capacitor size, and the transferred power to the grid (Yang et al., 2013). Increasing the dc-link voltage reduces the voltage ripple but increases the stresses on the power devices, the switching losses, and the higher frequency ripple in the output current. On the other side, reducing the dc-link capacitor size for saving costs increases the dc-link voltage ripple. The double grid-frequency voltage ripple has undesirable effects on the current controller of the inverter, the voltage controller of the dc-link voltage, and the efficiency of the MPPT controller. One issue caused by this double grid-frequency voltage ripple is harmonic distortion in the output current. These harmonics have a large impact on the power quality, operational efficiency, and reliability of the power system, loads, and protective relaying (Jain and Singh, 2011; Larose et al., 2013). Many standards as IEEE 929 and IEEE 1547 state that total harmonic distortion in the injected current to the grid from distributed generation must be less than 5% (Zhou et al., 2012). To compensate the dc-link voltage ripple effects a PWM control method is introduced in Enjeti and Shireen (1992). This control method feed forward the dc-link information to compensate the ripple effects. A control technique that allows for 25% ripple voltage without distorting the output current waveform is proposed in Brekken et al. (2002). Where the sampling frequency of the DC voltage controller output is 10 Hz. This technique leads to attenuate the voltage ripple in the control loop, but the system dynamic performance is degraded. Higher bandwidth for the voltage control loop is proposed in Ninad and Lopes (2012). Proportional resonant controller with a modified carrier signal is proposed in Darwish et al. (2011) to mitigate the oscillation effect on the dc-link voltage. Double grid-frequency ripple on the dc-link leads to ripple in the PV output voltage in single-phase grid-connected systems. As a result of voltage ripples on the dc-link voltage on the output of the boost converter, the boost converter input voltage may contain ripples too. In this case, the extracted power from the PV will contain ripple which leads to power loss due to inaccurate MPP operation unless the MPPT controller is well designed.

This paper proposes new control scheme for single-phase two-stage photovoltaic grid-connected system. The paper introduces solutions toward mitigate the side effects of the double grid-frequency voltage ripple on the transferred power quality and the operational efficiency of single-phase two-stage grid-connected PV system. The system has three control loops: MPPT control loop, dc-link voltage control loop and inverter current control loop. Solutions are introduced for all the three control loops in the system.

2. System configuration

The single-phase two-stage photovoltaic grid-connected system with its control is shown in Fig. 1. The system contains three controllers. The H-bridge inverter is controlled by a dual-loop controller. The outer loop controls the dc-link voltage to follow the reference value (V_{ref}) and generate the peak value (I_{ref}) of the reference current (i_{ref}) for the inner loop. For unity power factor operation, I_{ref} is multiplied by a unit-amplitude sinusoidal signal which is in phase with the grid voltage. A phase-locked loop (PLL) is used to obtain this signal. The current control loop regulates the inverter current (i) according to the reference current (i_{ref}). A MPPT controller is used to extract the available maximum power from the PV array.

2.1. Source of the double grid-frequency ripple

For unity power factor operation and based on Fig. 1, the inverter output power can be calculated as follows:

$$v_a = V_m \sin \omega t \quad (1)$$

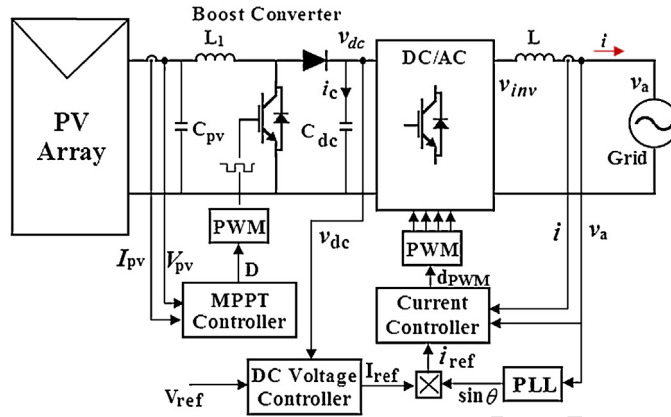


Fig. 1. Proposed single-phase two-stage grid-connected PV system.

$$i = I_m \sin \omega t \quad (2)$$

So,

$$P_o = V_m I_m \sin^2 \omega t \quad (3)$$

$$P_o = \frac{V_m I_m}{2} (1 - \cos 2\omega t) = \frac{V_m I_m}{2} - \frac{V_m I_m}{2} \cos 2\omega t \quad (4)$$

The first term of Eq. (4) is the average AC power injected to grid, while the second term represents the oscillations of the AC power which is the source of the double grid-frequency ripple. On the other hand, the inverter input power can be calculated as follows (3):

$$P_{in} = P_{pv} - i_c v_{dc} \quad (5)$$

$$P_{in} = P_{pv} - C_{dc} V_{dc} \frac{d\tilde{v}_{dc}}{dt} \quad (6)$$

Assuming one hundred percent of the inverter efficiency, then:

$$P_{in} = P_o \quad (7)$$

$$P_{pv} = \frac{V_m I_m}{2} \quad (8)$$

$$\frac{d\tilde{v}_{dc}}{dt} = \frac{V_m I_m}{2C_{dc} V_{dc}} \cos 2\omega t \quad (9)$$

then,

$$\tilde{v}_{dc} = \frac{V_m I_m}{4\omega C_{dc} V_{dc}} \sin 2\omega t = V_{rip} \sin 2\omega t \quad (10)$$

It is obvious from (10) that the dc-link voltage ripple \tilde{v}_{dc} depends on the inverter output power, the selected dc-link bus voltage V_{dc} , and the capacitor value C_{dc} . It is clear from (10) that as the capacitor value decreases, the voltage ripple increases.

2.2. Ripple voltage impacts on the inverter output power quality

For AC side of the inverter shown in Fig. 1, the following equation can be deduced:

$$L \frac{di}{dt} = v_{inv} - v_a \quad (11)$$

Based on (11), if v_{inv} or/and v_a contains any harmonics, it will propagate to the inverter output current, leading to a higher THD in the injected grid current and a poorer quality of the output power. Assuming that the grid voltage is

pure sinusoidal waveform, the harmonics induced by the inverter output voltage are dominant in the inverter output current. Based on Fig. 1, the inverter output voltage can be expressed as:

$$v_{inv} = d_{PWM} v_{dc} \quad (12)$$

This equation indicates that the output signal of the inverter current controller d_{PWM} , and the dc-link bus voltage determine the harmonics content of the inverter output voltage v_{inv} .

2.3. Ripple voltage impacts on the extracted PV power

Because of the presence of voltage ripples on the dc-link voltage on the output of the boost converter, the boost converter input voltage may contain ripples too. In this case, the extracted power from the PV will contain ripple which leads to power loss due to inaccurate MPP operation. The following analysis shows the effects of the double grid frequency voltage ripple on the extracted PV power.

The relation between the input and output voltages of the boost converter is well known as (Daniel, 2001):

$$v_{PV} = (1 - D)v_{dc} \quad (13)$$

where v_{PV} and v_{dc} are the input and output voltages of the boost converter, respectively. The MPPT controller output signal D is the duty ratio of the boost converter. It is clear from (13) that v_{PV} will contain the same ripple of v_{dc} if the duty ratio is a constant value. In this case:

$$v_{PV} = (1 - D)v_{dc} = (1 - D)V_{dc} + (1 - D)\tilde{v}_{dc} \quad (14)$$

$$v_{PV} = (1 - D)V_{dc} + (1 - D)V_{rip} \sin 2\omega t \quad (15)$$

$$v_{PV} = V_{pv} + \tilde{v}_{pv} \quad (16)$$

If V_{pv} is the PV voltage at MPP (V_{mp}), then, the PV current will have ripples around its maximum power point value I_{mp} such as:

$$i_{pv} = I_{mp} + \tilde{i}_{pv} \quad (17)$$

The PV output power in this case can be calculated as follows:

$$p_{pv} = (V_{mp} + \tilde{v}_{pv})(I_{mp} + \tilde{i}_{pv}) \quad (18)$$

$$p_{pv} = V_{mp}I_{mp} + V_{mp}\tilde{i}_{pv} + I_{mp}\tilde{v}_{pv} + \tilde{v}_{pv}\tilde{i}_{pv} \quad (19)$$

By equating the two middle terms of (19) to zero, the ripple component of the PV current can be obtained as follows:

$$V_{mp}\tilde{i}_{pv} + I_{mp}\tilde{v}_{pv} = 0 \quad (20)$$

$$\tilde{i}_{pv} = -\frac{I_{mp}}{V_{mp}}\tilde{v}_{pv} \quad (21)$$

$$\tilde{i}_{pv} = -\frac{I_{mp}}{V_{mp}}(1 - D)V_{rip} \sin 2\omega t \quad (22)$$

Accordingly, the extracted power is:

$$p_{pv} = V_{mp}I_{mp} + \tilde{v}_{pv}\tilde{i}_{pv} \quad (23)$$

From (15) and (22),

$$p_{pv} = V_{mp}I_{mp} - \frac{I_{mp}}{V_{mp}}(1 - D)^2 V_{rip}^2 \sin^2 2\omega t \quad (24)$$

This equation indicates that p_{pv} has an average value which is less than the maximum power value. From (24), as the double grid frequency voltage ripple increases, the extracted average PV power decreases. Also, the average value of this equation forces the MPPT controller to output a constant value of the duty ratio D .

3. Design of the proposed controllers

This paper introduces solutions toward mitigate the side effects of the double-grid frequency voltage ripple on the transferred power quality and the operational efficiency of single-phase two-stage grid-connected PV system. Solutions are introduced for all the three controllers in the system. In the MPPT control loop, the duty ratio control signal of the boost converter is modified to fully maximize the extracted PV power by reducing the PV voltage and current fluctuations. The contribution of the dc-link voltage control loop is in the controller design and calculations of its parameters to cancel out the double-grid frequency ripple effects and produces almost pure dc output signal as a reference for the inverter current controller. In the current control loop, a deadbeat current controller is used to obtain a modulating signal required to control the inverter power switches and produces the inverter output voltage. Details about these controllers are discussed in the following sections.

3.1. The inverter current controller

The single-phase H-bridge voltage source inverter can be controlled using two PWM switching strategies, namely bi-level and tri-level (Atia and Salem, 2013). In the bi-level switching strategy, the inverter output voltage is switching between the positive and negative inverter input dc source, while in the tri-level switching strategy, the inverter output voltage is switching between the positive (or negative) inverter input dc source and zero voltage.

The proposed current controller in this paper is used to calculate the inverter output voltage required to force the actual inverter current (i) to follow the reference current (i_{ref}). The difference between i_{ref} and i is the current error (i_{err}).

In tri-level operation, the following equations are valid (Atia and Salem, 2013):

$$\frac{di_1}{dt} = \frac{v_{dc} - v_a}{L} \quad (25)$$

$$\frac{di_2}{dt} = \frac{0 - v_a}{L} \quad (26)$$

where di_1/dt and di_2/dt are the rate of change of the inverter current (i) during T_{on} and T_{off} time periods of the inverter switches respectively, v_a is the grid voltage, and v_{dc} is the dc-link voltage. To compensate the current error during a switching time period T , the following equation can be used:

$$i_{err} = \frac{di_1}{dt} T_{on} + \frac{di_2}{dt} T_{off} \quad (27)$$

For a constant switching frequency the switching time period T is:

$$T = T_{on} + T_{off} \quad (28)$$

From Eqs. (25–28), T_{on} can be calculated as follows:

$$T_{on} = \frac{T((L/T)i_{err} + v_a)}{v_{dc}} \quad (29)$$

Then the required modulating signal can be obtained as:

$$d_{PWM} = \frac{T_{on}}{T} = \frac{((L/T)i_{err} + v_a)}{v_{dc}} \quad (30)$$

The obtained modulating signal is used to generate the PWM signals required to control the inverter switches and to determine the inverter output voltage which is represented by the following equation:

$$v_{inv} = v_{dc} d_{PWM} = \frac{L}{T} i_{err} + v_a \quad (31)$$

Based on (31), the dc-link voltage has no effect on the inverter output where the modulating signal d_{PWM} canceled out the effect of dc-link voltage. Consequently, the dc-link voltage has no effect on the THD of the output current. The THD of the output current depends on the current reference signal only and this is a contribution of the proposed inverter current controller toward mitigation of the effects of the dc-link double grid frequency voltage ripple.

Table 1
Results of the proposed current controller.

V_{rip}	I_{rip}	THD in the current	
		i_{ref}	i
0%	0%	0%	1.38%
5%	0%	0%	1.38%
0%	5%	1.27%	1.99%
5%	5%	1.27%	1.99%

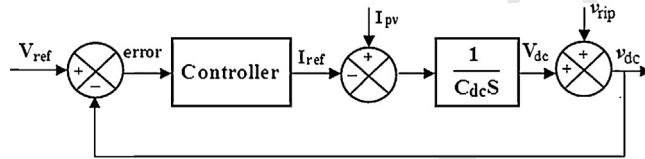


Fig. 2. The dc-link voltage controller block diagram.

3.1.1. Performance evaluation of the proposed current controller

A MATLAB/Simulink model is designed to study only the impact of the dc-link voltage ripple and the reference current THD on the performance of the proposed current controller away from the PV array. In this model, a controlled voltage source is used to simulate the dc-link voltage waveforms with different ripple values. Also, a signal generator is used to generate the reference current (i_{ref}) with different THD values. Table 1 shows the obtained results which indicate the influences of V_{rip} and I_{rip} on THD of the inverter output current. The results are taken in case of the peak value of the reference current is 60 A and grid interface inductance (L) is 2 mH.

Results presented in Table 1 clearly show that the THD of the inverter output current is affected only by THD of the reference signal i_{ref} . The obtained results ensure that the dc-link voltage ripple has no effect on the THD of the output current.

3.2. DC bus voltage controller

Based on (10) and after designing the system, v_{rip} is determined by the inverter output power. These ripples will propagate to the input of the dc-link voltage controller and penetrate to the controller output. Having these ripples on the dc-link voltage controller output deteriorates the quality of the inverter output power as discussed in the previous section. In this section it is proposed to design a dc-link voltage controller which is able to cancel out the double grid-frequency ripple effects and produces almost pure dc output signal as a reference for the inverter current controller.

The block diagram for controlling the dc-link voltage is shown in Fig. 2. The design of the proposed voltage controller is accomplished in two stages.

The first stage depends on the classical controller suggested in Salem (2008). The block diagram of the proposed controller in its first stage is shown in Fig. 3. The purpose of this stage is to obtain a fast and critically damped response of the controlled voltage.

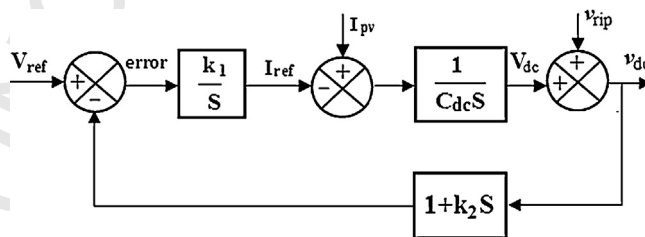


Fig. 3. The proposed dc-link voltage controller in its first stage.

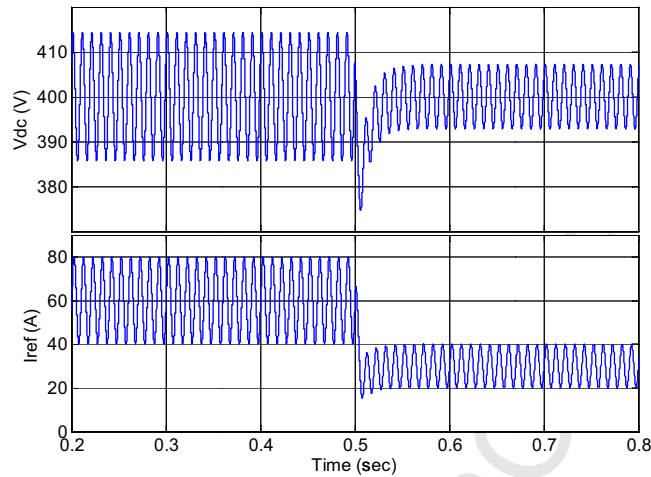


Fig. 4. The first stage dc-link voltage controller performance.

Based on Salem (2008), the controller parameters k_1 and k_2 can be calculated as follows:

$$k_2 = 2\sqrt{\frac{C_{dc}\eta}{k_1}} \quad (32)$$

$$k_1 * k_2 = \frac{\Delta I_{pv}}{V_{dip}} \quad (33)$$

where η is the damping factor, and V_{dip} is the defined maximum dip in the dc-link voltage due to a defined maximum step change of the PV output current ΔI_{pv} . A MATLAB/Simulink model of the block diagram shown in Fig. 3 is designed to simulate the transient performance of the dc-link voltage controller according to a step change in the PV current. As shown in Fig. 4 (upper plot), the dc-link voltage is settled down in about 0.04 s after the step change of the PV current from 60 A to 30 A at time $t=0.5$ s. This is a contribution for the dc-link voltage controller. As shown in Fig. 4, (lower plot), the controller output signal (I_{ref}) has a higher double grid frequency ripple. So, the second stage of the voltage controller is designed to cancel out this ripple.

The complete design of the proposed voltage controller with its second stage is shown in Fig. 5, where a derivative branch is added in parallel with the integral branch. The purpose of the derivative branch is to cancel out the steady state ripple found in the error signal. For this reason, the derivative parameter k_d is suggested to be calculated as presented next.

During steady state operation, the controller error signal must have the following form:

$$error = A_1 \cos(2\omega t) \quad (34)$$

Then the controller integrator output signal is:

$$Integrator_output = k_1 \int A_1 \cos(2\omega t) dt = \frac{k_1 A_1}{2\omega} \sin(2\omega t) \quad (35)$$

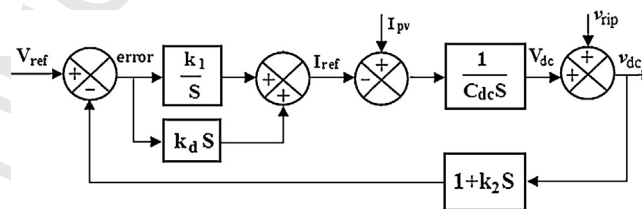


Fig. 5. Complete design of the proposed dc-link voltage controller.

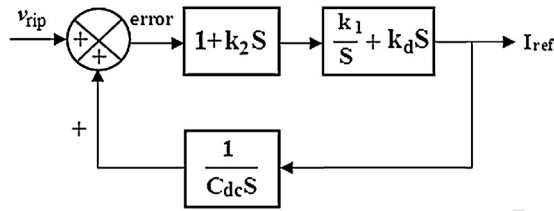


Fig. 6. Block diagram of the relation between I_{ref} and \tilde{v}_{dc} .

The derivative output signal is:

$$Derivative_output = k_d \frac{d}{dt}(A_1 \cos(2\omega t)) = -2\omega k_d A_1 \sin(2\omega t) \quad (36)$$

To cancel out the ripple in the voltage controller output, the summation of the integrator output in (35) and the derivative output in (36) must be equal to zero. Hence:

$$k_d = \frac{k_1}{4\omega^2} \quad (37)$$

The block shown in Fig. 5 is redrawn as shown in Fig. 6 to find a relation between the controller output I_{ref} and the dc link double grid-frequency voltage ripple \tilde{v}_{dc} .

The block diagram shown in Fig. 6 has the following transfer function:

$$\frac{I_{ref}(s)}{\tilde{v}_{dc}(s)} = \frac{G(s)}{1 - G(s)H(s)} \quad (38)$$

where:

$$G(s) = (1 + k_2 s) \left(\frac{k_1}{s} + k_d s \right) \quad (39)$$

$$H(s) = \frac{1}{C_{dc} s} \quad (40)$$

The Bode diagram of (38) is shown in Fig. 7. The gain at the double grid-frequency is about (-300 dB) which means that the input signal with this frequency has no effect on the output signal. This result demonstrates the effectiveness of the proposed voltage controller to cancel out the effects of the double grid frequency voltage ripple on the system performance.

The transient performance of the dc-link voltage controller in its final form according to a step change in the PV current is shown in Fig. 8. The dc-link voltage response is shown in Fig. 8 (upper plot). As shown in Fig. 8 (lower

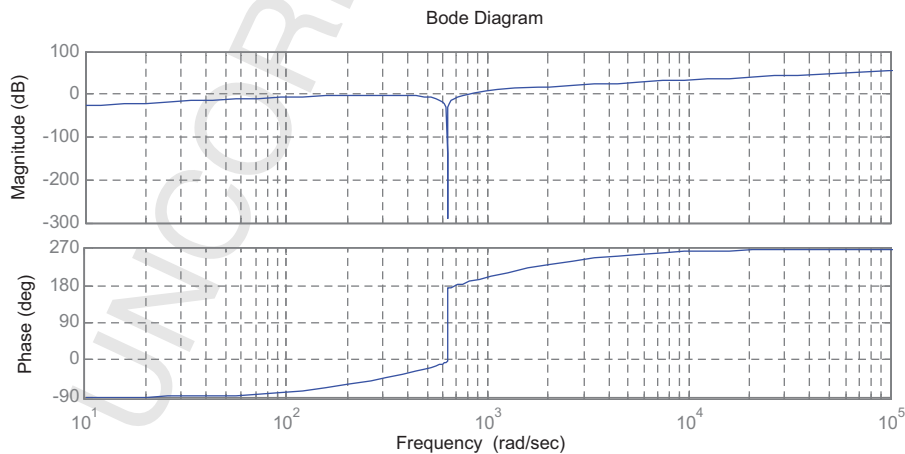


Fig. 7. Bode diagram of the dc-link voltage controller.

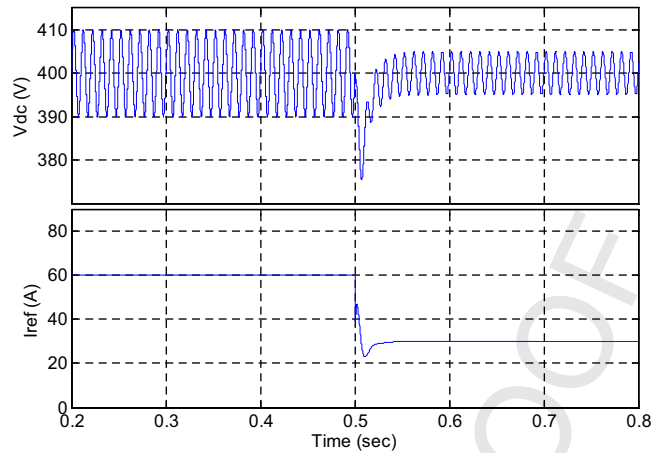


Fig. 8. dc-link voltage controller performance with $C_{dc} = 4000 \mu\text{F}$.

228 plot), the controller output is almost a constant dc value, which is the main contribution of the voltage controller toward
229 enhancing the quality of the transferred power.

230 **3.3. The maximum power point tracking controller**

231 Many MPP tracking methods have been developed and implemented in the literatures. In this paper it is proposed
232 to use the incremental conductance methods for the MPPT controller. The incremental conductance (Esram, 2007) is
233 based on the fact that the slope of the PV array power curve is zero at the MPP, positive on the left of the MPP, and
234 negative on the right of the MPP as shown in Fig. 9. The PV current and voltage are the input signals of the incremental
235 conductance method.

236
$$\frac{dP}{dV} = 0 \quad \text{at MPP} \tag{41}$$

237
$$\frac{dP}{dV} = \frac{d(IV)}{dV} = I + V \frac{dI}{dV} = 0 \tag{42}$$

238
$$\frac{dI}{dV} = \frac{-I}{V} \tag{43}$$

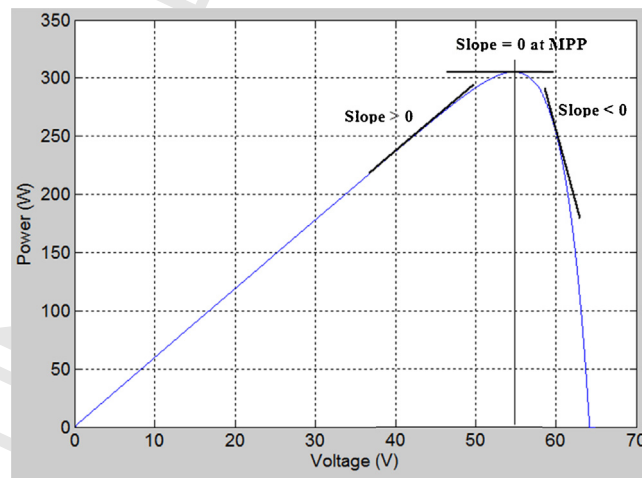


Fig. 9. The slope of P - V curve with respect to MPP for one module.

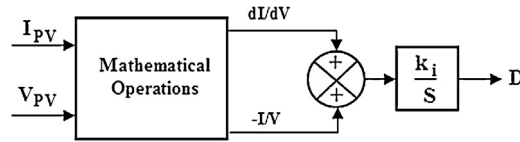


Fig. 10. Block diagram of MPPT controller.

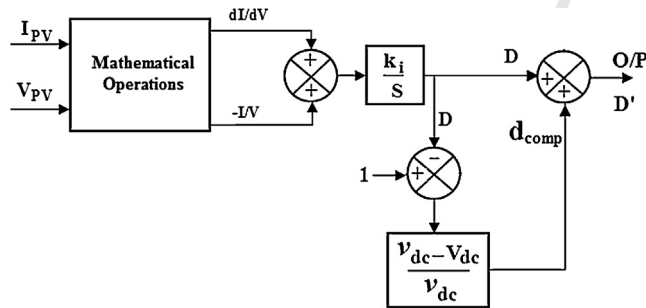


Fig. 11. Modified MPPT controller.

$$\frac{\Delta I}{\Delta V} = \frac{-I}{V} \tag{44}$$

The MPP can thus be tracked by summing the instantaneous conductance ($-I/V$) to the incremental conductance ($\Delta I/\Delta V$) to obtain an error signal. Then an integrator receives this error signal and generates the duty ratio D , which is the output of the MPPT controller as shown in Fig. 10. A PWM module is used to transfer the duty ratio D into pulses required to control the boost converter switch. As discussed in Section 2.3, the double grid frequency ripple propagates to the PV voltage and current which leads to extract an average power less than the maximum value. The extracted average power forces the MPPT controller to output a constant duty ratio. To compensate the effects of the double grid frequency voltage ripple on the performance of the MPPT controller, it is proposed to add a compensating signal d_{comp} to the controller output duty ratio D . This compensating signal is required to cancel out the ripple reflected on the PV voltage found in (15).

By adding the compensating signal d_{comp} to the duty ratio D in (15), it becomes as follows:

$$v_{PV} = (1 - (D + d_{comp})) * V_{dc} + (1 - (D + d_{comp})) * V_{rip} \sin 2\omega t \tag{45}$$

$$v_{PV} = (1 - D) * V_{dc} + (1 - D) * V_{rip} \sin 2\omega t - d_{comp}(V_{dc} + V_{rip} \sin 2\omega t) \tag{46}$$

To cancel out the PV voltage ripple, the summation of the second and third terms in the preceding equation must equal to zero, then:

$$d_{comp} = \frac{(1 - D) * V_{rip} \sin 2\omega t}{V_{dc} + V_{rip} \sin 2\omega t} \tag{47}$$

$$d_{comp} = (1 - D) \frac{v_{dc} - V_{dc}}{v_{dc}} \tag{48}$$

$$D' = D + d_{comp} \tag{49}$$

The modified duty ratio D' enters to modulator to generate PWM signal to the boost converter. The modified MPPT controller for enhancing the extracted PV power is shown in Fig. 11 which is another contribution in this paper.

4. System simulation

The proposed system is designed to transfer 10 kW from the PV array to the grid. The grid voltage is 220 V at 50 Hz. Sunpower 305 W module is chosen to construct the PV array. The photovoltaic array is composed of 33 modules of 305 W each. The modules arranged in 11 parallel strings with 3 modules in series in each string. The open circuit

Table 2

Q5 PV module and array ratings.

STC at 1000 W/m ² , 25 °C	Module rating	Array rating
V_{oc}	64.2 V	192.6 V
I_{sc}	5.96 A	65.56 A
V_{mp}	54.7 V	164.1 V
I_{mp}	5.58 A	61.38 A
P_{max}	305 W	10.065 kW

Table 3

Parameters for boost converter design.

V_{mp}	164.2 V	P_{out}	10 kW
D	0.5895	f	50 Hz
ΔI_L	5 A	V_{dc}	400 V
f_{sw}	10 kHz	V_{rip}	5%

Table 4

The parameters of the three controllers.

MPPT controller	Voltage controller ($\Delta I_{pv}/V_{dip} = 30 \text{ A}/20 \text{ V}$)			Current controller
k_i	k_1	k_2	k_d	L
7	140	106×10^{-3}	3.55×10^{-4}	2 mH

voltage of the string is 192.6 V. The short circuit current of the array is 65.56 A. The total STC power of the array is 10.065 kW with maximum power point voltage of 164.2 V and current of 61.38 A.

The rated values of the PV module and array are summarized in Table 2.

Parameters for boost converter design are shown in Table 3. The boost converter inductance is designed based on the following equation (Daniel, 2001):

$$L_1 = \frac{V_{mp} * D}{\Delta I_L f_{sw}} \quad (50)$$

From Du et al. (2015):

$$C_{dc} = \frac{P_{out}}{2\pi f V_{dc} V_{rip}} \quad (51)$$

From the system rating and selected voltage and current ripples, and based on (50) and (51) the values of the inductance L_1 and capacitor C_{dc} are:

$$L_1 = 2 \text{ mH}, \quad C_{dc} = 4000 \text{ } \mu\text{F}$$

The parameters of the proposed three controllers are shown in Table 4.

The proposed system is simulated with the components and parameters mentioned above.

5. Simulation results

A MATLAB/Simulink program model is designed to simulate the complete system of the single-phase two-stage photovoltaic grid-connected system which is shown in Fig. 1.

Fig. 12 indicates the system performance with the proposed three controllers. From top to bottom: grid voltage and current, dc-link voltage and average PV power. In Fig. 12, 50–100% sun insolation step change occurred at time $t = 0.5 \text{ s}$. In the upper plot of Fig. 12, the unity power factor operation can be noticed where the injected grid current is in phase with grid voltage. THD of the output current is about 2.38% and 1.3% at 50% and 100% insolation levels,

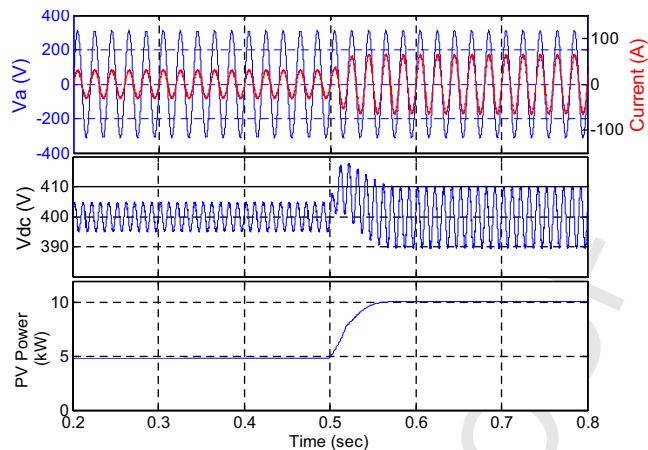


Fig. 12. System performance with step change in insolation level.

283 respectively. In the middle of Fig. 12 the dc-link voltage has 2.5% peak to peak voltage ripple while transferring a
 284 power of 5 kW and the voltage ripple increased to 5% when the output power increased to 10 kW as stated in (51). The
 285 superiority of the voltage controller performance to stabilize the dc-link voltage in about 0.05 s after step change in
 286 insolation level from 50% to 100% is clear in middle of Fig. 12. The maximum power from the PV array is extracted
 287 in each case (50% and 100% insolation) as presented in the bottom of Fig. 12.

288 In Fig. 13 a zoom in is done for the upper plot of Fig. 12 to clearly shows the step change response of the current
 289 controller at $t=0.5$ s. From Fig. 13, it can be depicted that the current controller has the ability to change the output
 290 current fast and smoothly from 32 A to 64 A peak values.

291 Fig. 14 shows the transient response of dc-link voltage controller output signal due to a 50% increase of the PV
 292 power. In spite of the ripple found on the dc-link voltage as shown in Fig. 14, the controller output is almost dc signal
 293 which leads to minimization of the output current THD.

294 Fig. 15 shows the effect of the modified MPPT controller on the extracted power from PV array. During the first
 295 half of Fig. 15, the MPPT controller without the compensation factor is applied, while in the second half, d_{comp} signal
 296 is added. In the first half of the figure the duty ratio D is constant and a double grid-frequency ripple penetrates to
 297 the PV voltage and current that decrease the extracted average power as analysed in Section 2.3. While in the second
 298 half, d_{comp} signal is added that leads to an oscillation-free operation in both of PV voltage and current. As shown in
 299 the second half of Fig. 15, there is increase of the extracted average PV power. The added compensation factor d_{comp}

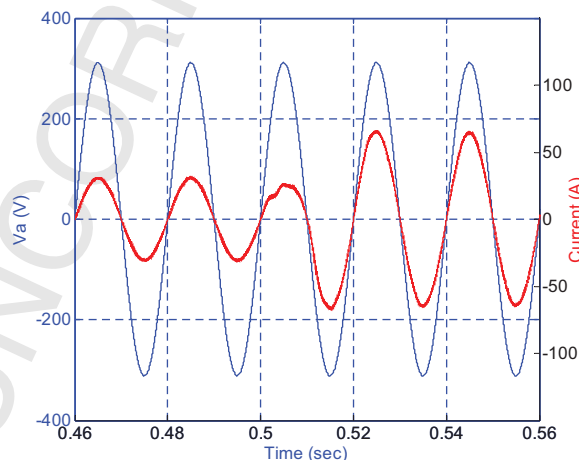


Fig. 13. Zoom in for grid voltage and injected current at unity power factor operation.

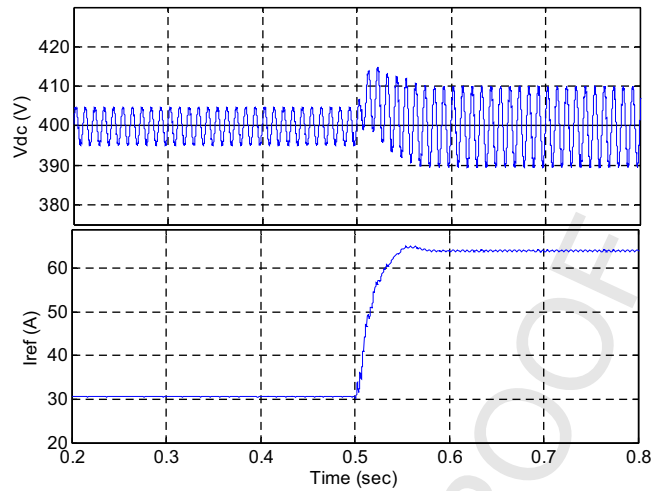


Fig. 14. dc-link voltage and voltage controller output.

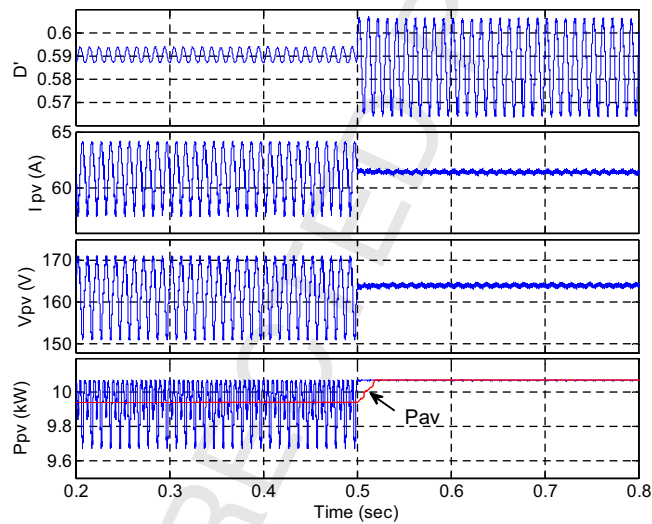


Fig. 15. Modified MPPT controller results.

300 makes the difference of the MPPT controller performance. The harmony between the system controllers leads to the
301 power quality insurance and total system efficiency occurrence.

302 6. Conclusions

303 In this paper, three controllers are proposed and designed for single-phase two-stage PV grid-connected system to
304 mitigate the double grid-frequency voltage ripple effects on the system performance. Based on a simple block diagram,
305 the dc-link voltage controller is designed and its parameters are calculated to provide critically damped response for
306 the dc-link voltage and to generate free-ripple reference signal for the inverter current controller. The design of the
307 inverter current controller is based on the deadbeat strategy to eliminate the dc-link voltage ripple effects on the THD
308 of the output current. To maximize the extracted PV power, the MPPT controller is modified by adding a compensating
309 signal which depends on the dc-link voltage ripple. Simulation results show high quality performance of the control
310 system where the output AC power quality is achieved and higher efficiency of the overall system is gained.

311 **Q3** **Uncited reference**

312 Libo et al. (2007).

313 **References**

- 314 Atia, Y., Salem, M., 2013. Microcontroller-based improved predictive current controlled VSI for single-phase grid-connected systems. *J. Power*
315 *Electron.* 13 (6).
- 316 Ahmed, M., Orabi, M., AbdelRahim, O., 2013. Two-stage micro-grid inverter with high-voltage gain for photovoltaic applications. *IET Power*
317 *Electron.* 6 (9), 1812–1821.
- 318 Brekken, T., Bhiwapurkar, N., Rathi, M., Mohan, N., Henze, C., Moumneh, L.R., 2002. Utility-connected power converter for maximizing power
319 transfer from a photovoltaic source while drawing ripple-free current. In: *Proc. IEEE 33rd Annu. Power Electronics Specialists Conf. (PESC)*,
320 pp. 1518–1522.
- 321 Darwish, A., Abdelsalam, A.K., Massoud, A.M., Ahmed, S., 2011. Single phase grid connected current source inverter: mitigation of oscillating
322 power effect on the grid current. In: *Proc. IET Renewable Power Generation (RPG)*, pp. 1–7.
- 323 Daniel, H., 2001. *Power Electronics*. McGraw-Hill, New York.
- 324 Du, Y., Xiao, W., Hu, Y., Lu, D.D.-C., 2014. Control approach to achieve burst mode operation with DC-link voltage protection in single-phase
325 two-stage PV inverters. In: *IEEE Energy Conversion Congress and Exposition (ECCE)*, Pittsburgh, PA.
- 326 Du, Y., Lu, D.D.-C., Chu, G.M.L., Xiao, W., 2015. Closed-form solution of time-varying model and its applications for output current harmonics
327 in two-stage PV inverter. *IEEE Trans. Sustain. Energy* 6 (1).
- 328 Enjeti, P.N., Shireen, W., 1992. A new technique to reject dc-link voltage ripple for inverters operating on programmed PWM waveforms. *IEEE*
329 *Trans. Power Electron.* 7 (1), 171–180.
- 330 ESRAM, T., 2007. Comparison of photovoltaic array maximum power point tracking techniques. *IEEE Trans. Energy Convers.* 22 (2).
- 331 Jain, S.K., Singh, S.N., 2011. Harmonics estimation in emerging power system: key issues and challenges. *Electr. Power Syst. Res.* 81 (9), 1754–1766.
- 332 Lal, V., Siddhardha, M., Singh, S.N., 2013. Control of a large scale single-stage grid-connected PV system utilizing MPPT and reactive power
333 capability. In: *IEEE Power and Energy Society General Meeting (PES)*.
- 334 Larose, C., Gagnon, R., Prud'Homme, P., Fecteau, M., Asmine, M., 2013. Type-III wind power plant harmonic emissions: field measurements and
335 aggregation guidelines for adequate representation of harmonics. *IEEE Trans. Sustain. Energy* 4 (3), 797–804.
- 336 Libo, W., Zhengming, Z., Jianzheng, L., 2007. A single-stage three-phase grid-connected photovoltaic system with modified MPPT method and
337 reactive power compensation. *IEEE Trans. Energy Convers.* 22 (4).
- 338 **Q4** Ninad, N.A., Lopes, L.A.C., 2012. A low power single-phase utility interactive inverter for residential PV generation with small dc link. *Electr.*
339 *Power Compon. Syst.*
- 340 Salem, M.M., 2008. Classical controller with intelligent properties for speed control of vector controlled induction motor. *J. Power Electron.* 8 (3),
341 210–216.
- 342 Yang, C., Smedley, K., 2008. Three-phase boost-type grid-connected inverter. *IEEE Trans. Power Electron.* 23 (5).
- 343 Yang, Y., Zhou, K., Blaabjerg, F., 2013. Harmonics suppression for single-phase grid-connected PV systems in different operation modes. In:
344 *Twenty-Eighth Annual IEEE Applied Power Electronics Conference and Exposition (APEC)*.
- 345 Wang, Z., Xiao, L., Zhang, J., Huang, Y., Yao, Z.-L., Yan, Y.-G., 2007. Design of a two-stage fuel cell based single-phase utility-interactive inverter.
346 In: *IEEE Power Electronics Specialists Conference*, pp. 1227–1231.
- 347 Zhou, K., Qiu, Z., Yang, Y., 2012. Current harmonics suppression of single phase PWM rectifiers. In: *Proc. of PEDG'12*, pp. 54–57.